

pubs.acs.org/acsapm Article

# Thermal Conductivity of Pentiptycene-Based Poly(o-hydroxyimide) Copolymers: A Study via Integrated Experiments and Simulations

Xingfei Wei, Zihan Huang, Stephen Koch, Massimiliano Zamengo, Yichen Deng, Marilyn L. Minus, Junko Morikawa, Ruilan Guo, and Tengfei Luo\*



Cite This: ACS Appl. Polym. Mater. 2021, 3, 2979–2987



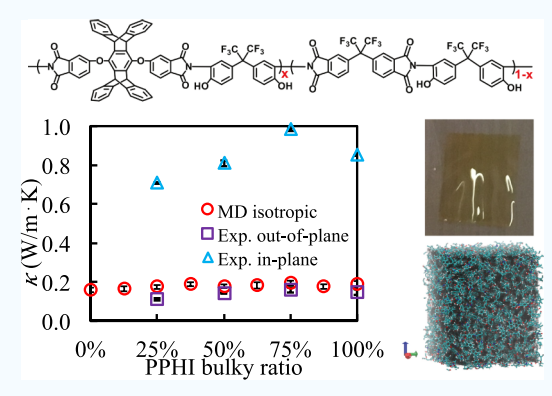
ACCESS

Metrics & More

Article Recommendations

Supporting Information

ABSTRACT: Polymers play important roles in thermal transport applications, and conjugated polymers have been identified as promising candidates to achieve high thermal conductivity. In this paper, pentiptycene-based poly(o-hydroxyimide) (PPHI)-conjugated copolymers, made of a bulky pentiptycene segment and a -CF<sub>3</sub> substituent segment, with different segment ratios are studied. Both experimental and molecular dynamics (MD) simulation results show that polymer thermal conductivity increases as the ratio of the bulky segment increases. The experimental in-plane thermal conductivity is significantly higher than the out-of-plane value (up to 6.38 times), which is due to the chain alignment effect in the in-plane direction. The highest measured in-plane thermal conductivity reaches 0.982 W/m·K, which is among the highest in polymer thermal conductivity. Experimental results show that the volumetric heat capacity increases with the bulky segment ratio which should have a positive impact on the thermal conductivity. MD results further



show that the bulky segment helps increase the spatial extension of polymer chains and the amount of strong interatomic forces related to the aromatic carbon atoms, both leading to increasing thermal conductivity. In addition, we also find that the fractional free volume in the PPHI copolymers decreases as the bulky segment ratio increases, which should also have contributed to the increase in thermal conductivity.

KEYWORDS: thermal conductivity, polyimide, π-stacking conjugation, pentiptycene-based poly(hydroxyimide), fractional free volume

# INTRODUCTION

The thermal conductivity of polymers is critical to many applications, such as electronics, functional composite materials, and energy conversion. <sup>1-7</sup> The mechanism of heat transfer in polymers depends on a variety of factors like chain conformation, electrostatic interactions, and intra- and interchain interactions.<sup>8–13</sup> In 2010, Shen et al. discovered that ultradrawn crystalline polyethylene (PE) nanofibers could have thermal conductivity as high as 104 W/m·K, 14,15 which is up to 3 orders of magnitude larger than that of amorphous polymers (0.1–0.7 W/m·K). 11,16–18 Simulations have found that in polymers, thermal transport along the chain backbone is very efficient due to strong covalent bonding interactions. In contrast, heat transfer between chains is generally inefficient because of the weak nonbonding interactions. 6,10,16 A number of studies have shown a strong correlation between polymer chain conformation and thermal conductivity. 8,10,20 For example, in polymer nanofibers, stretching the polymer backbone to suppress the segmental rotation around the backbone dihedral angle can significantly enhance heat transfer in the backbone direction. 6,9,21-23 It is also found that in amorphous polymers, thermal conductivity is directly related to the chain length <sup>12,24,25</sup> and chain stiffness. <sup>10,19,26</sup> In general, heat transfer in polymers is dominated by the strong bonding interactions, and if a polymer chain is more spatially extended, its thermal conductivity will be higher. <sup>10,27</sup> A spatially extended chain can be achieved by many means, such as mechanically stretching the polymer chain, chemically synthesizing a rigid rodlike backbone, or engineering proper sidechains. <sup>10,19,28</sup> Polymers with a conjugated backbone are expected to be more thermally conductive since they tend to be stiffer. For example, it is reported that nanofibers of conjugated polymer have more rigid backbones and thus higher thermal conductivity. <sup>29–31</sup> It is also reported that due to the molecular level chain alignment, amorphous polythiophene nanofibers, which are conjugated polymers, fabricated by nanotemplating can reach ~4.4 W/m·K. <sup>32</sup> However, in the bulk amorphous phase, most conjugated polymers are in the range of 0.1–0.4 W/m·K. <sup>28,33</sup> A previous experimental study

Received: January 28, 2021 Accepted: May 4, 2021 Published: May 18, 2021





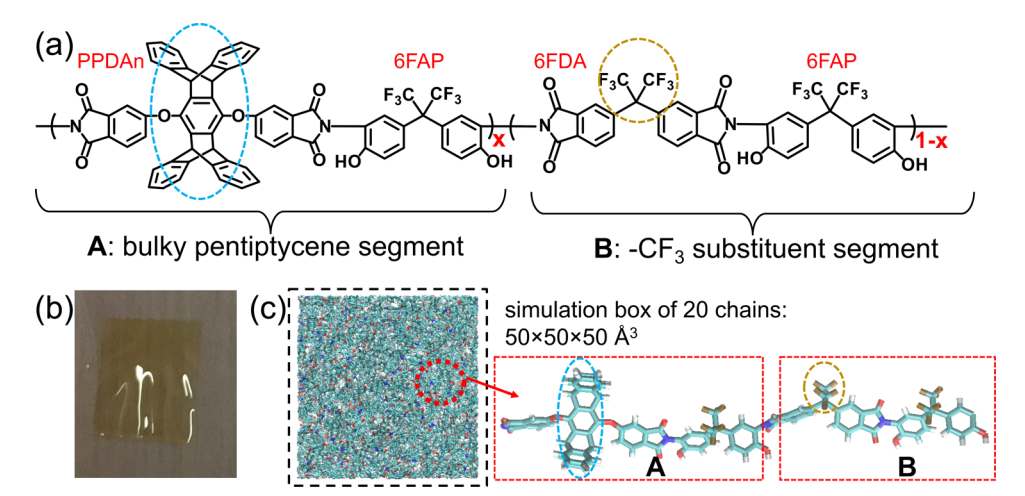


Figure 1. (a) Chemical structure of PPHI copolymers with the bulky pentiptycene-based segment and the CF3-based segment in various ratios (x). (b) Picture of a representative polymer thin film. (c) MD simulation model for PPHI copolymers.

showed that with a long linear sidechain, thermal conductivity of a conjugated polymer could be increased by 160% over its counterpart with a bulkier sidechain from 0.1 to 0.26 W/m· K,28 but this is much lower than 4.4 W/m·K achieved from nanotemplating.<sup>32</sup> Meanwhile, taking advantage of both the conjugated backbone and strong  $\pi - \pi$  stacking interactions, researchers reported that amorphous poly(3-hexylthiophene) could reach a thermal conductivity value of ~2.2 W/m·K.<sup>34</sup> However, such high thermal conductivity values (4.4 and 2.2 W/m·K) are not common, and the heat-transfer mechanism in amorphous polymers with strong conjugated  $\pi$ - $\pi$  stacking interactions remains to be further elucidated.

Aromatic poly(hydroxyimide)s are rigid polymers widely used in gas separation membranes.  $^{35-39}$  The chain stiffness and porosity of aromatic poly(hydroxyimide)s can be tuned by different substituent groups on the two monomers, namely, the aromatic dianhydride and the aromatic diamine. 36 In pentiptycene-based poly(o-hydroxyimide) (PPHI), the chain stiffness and the fractional free volume (FFV) (or microporosity) can be tuned by different ratios of the pentiptycenecontaining segment and the -CF3 substituent segment (e.g., Figure 1a).<sup>37</sup> Such tunability may provide a means to help understand thermal transport in conjugated polymers. However, the thermal conductivity of the PPHI-type polymers has never been reported. Both the conjugated pentiptycene group and the -CF3 group can affect the polymer chain conformation and the bulk structure, such as radius of gyration  $(R_{\sigma})$  and porosity. In porous materials, porosity is a critical parameter to thermal conductivity as pores cannot transfer heat. Many studies have shown that the thermal conductivity decreases as the porosity increases. 40-42 It is also found that inhomogeneous porosity and a smaller pore size will further reduce the thermal conductivity. 42,43 A simulation model suggested that the thermal conductivity of a polymer foam can be as low as 0.015 W/m·K when its porosity is 85% and the pore size is 1 nm. 44 However, the combinational effects from the porosity and conjugated backbone on the thermal conductivity of microporous conjugated polymers have not been previously studied.

In this work, we study the thermal conductivity of a series of pentiptycene-based PPHIs with strong  $\pi-\pi$  stacking conjugation, which have a copolymer structure consisting of bulky pentiptycene-containing segments and -CF3-substituted segments (Figure 1a) in systematically varied ratios. Both experiments and molecular dynamic (MD) simulations are employed to explore the thermal transport mechanism. Thermal conductivity, heat capacity, density, and average speed of sound are experimentally measured. In the MD simulations, molecular-level details, including  $R_{e}$ , interatomic forces, and FFV, are analyzed together with the predicted thermal conductivity. Both experimental and MD simulation results show that the polymer thermal conductivity increases as the ratio of the bulky segment increases. The experimental inplane thermal conductivity is significantly higher than the outof-plane value (up to 6.38 times). Experimental results show that the volumetric heat capacity increases with the bulky segment ratio, which should have a positive impact on the thermal conductivity. MD results further show that the bulky segment helps increase the spatial extension of polymer chains and the amount of strong interatomic forces related to the aromatic carbon atoms, both of which can contribute to increasing thermal conductivity. In addition, we also find that the FFV in the PPHI copolymers decreases as the bulky segment ratio increases, which should also have contributed to the increase in thermal conductivity.

# **■ EXPERIMENTAL SECTION**

Materials. 4,4'-hexafluoroisopropylidene biphthalic dianhydride (6FDA) and 2,2'-bis(3-amino-4-hydroxyphenyl) hexafluoropropane (6FAP) were purchased from Akron Polymer Systems and dried under vacuum overnight before use. Pentiptycene-based dianhydride (PPDAn) was first prepared using our previously reported method.<sup>37–39</sup> Briefly, pentiptycene diquinone was prepared first via a Diels-Alder addition reaction, which was then reduced to pentiptycene diol. In the next step, the two hydroxyl groups were substituted by nitrile groups through a nucleophilic aromatic substitution reaction, followed by a hydrolysis step and then a dehydration reaction to afford the final anhydride structure. The obtained PPDAn was dried at 160 °C in vacuum overnight before use.<sup>37</sup>

Polymer Synthesis and Film Fabrication. PPHI copolymers (Figure 1a) were synthesized by condensation polymerization using PPDAn, 6FDA, and 6FAP in predetermined ratios. 38,39 pentiptycene-containing bulky segment ratio was tuned to be 25, 50, 75, and 100% by changing the molar ratios between PPDAn and 6FDA. For example, for a copolymer with the 25% pentiptycenebased segment, a molar ratio of PPDAn:6FDA:6FAP of 0.5:1.5:2 is used in the synthesis. The synthesis steps of PPHI-0.25 are as follows:

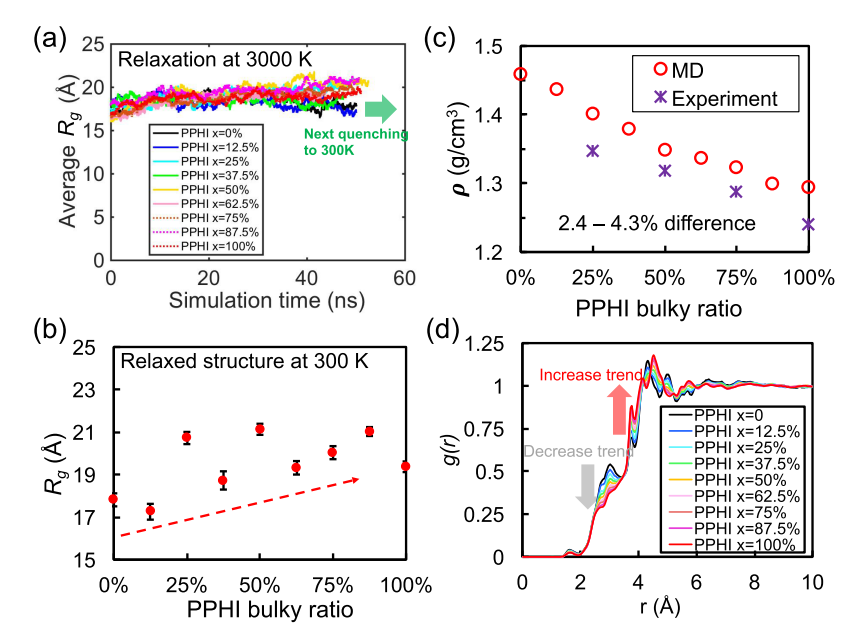


Figure 2. (a) Polymer chain conformation ( $R_g$ ) at 3000 K for relaxing more than 50 ns. (b) Final polymer chain  $R_g$  values at 300 K with different pentiptycene contents. (c) Final polymer densities at 300 K compared with experimental results. (d) RDF shows structures of PPHI block copolymers.

PPDAn (0.3 g) and 6FDA (0.5351 g) were added in the flask along with 4.2 mL of m-cresol and allowed to fully dissolve at 140 °C, followed by adding 6FAP (0.5867 g) with another 3 mL of m-cresol in a 100 mL flame-dried three-neck flask. The mixture was stirred under N<sub>2</sub> at room temperature overnight to form a poly(amic acid) intermediate. Then, a condenser was connected to the flask through a Dean-Stark trap, and 5 mL of toluene was added. The flask was heated to 190 °C and kept refluxing for 12 h, and during this step, water was removed azeotropically. 1:1 (v/v) water/methanol mixture was used to precipitate the polymer product. The polymer was washed in methanol and dried at 180 °C under vacuum overnight. The polymer film was fabricated by solution casting.<sup>37</sup> The freshly synthesized fibrous polymer was dissolved in anhydrous 1-methyl-2pyrrolidinone at  $\sim$ 7 wt % and filtered through a 0.45  $\mu m$ poly(tetrafluoroethylene) syringe filter. Then, the polymer solution was casted on a leveled glass plate and dried under an infrared lamp overnight (at ~70 °C). The final polymer thin film was peeled off and dried at 180 °C under vacuum overnight to remove the residual solvent. A representative sample picture is shown in Figure 1b.

**Polymer Characterization.** The specific heat capacity,  $c_n$ , was determined by differential scanning calorimetry analysis using a PerkinElmer Pyris 7 instrument. The polymer sample (0.3-0.8 mg) was used and heated from 20 to 40 °C at a heating rate of 10 °C/min and at a nitrogen purge rate of 50 mL/min. The specific heat capacity of the sample was determined using sapphire ( $\alpha$ -Al<sub>2</sub>O<sub>3</sub> single crystal) as a standard reference material based on the ISO11357-4 protocol. The Young's modulus was measured by a HR-2 Discover hybrid rheometer (TA Instruments) using the linear tension fixture. The anisotropic thermal diffusivities in the out-of-plane and in-plane (long axis) directions of the films were measured by temperature wave analysis methods, conforming to ISO22007-3, by using the ai-Phase mobile M3 type 1 and M10 type 2 systems by ai-Phase Co. Ltd Details of the thermal diffusivity measurement are Tokyo, Japan.43 included in the Supporting Information. Thermal conductivity ( $\kappa$ ) is calculated from thermal diffusivity ( $\alpha$ ) and specific heat capacity ( $c_p$ ) through the relation  $\kappa = \alpha \rho c_v$ , where density  $\rho$  was measured at room temperature by the buoyancy method via Archimedes' principle using an analytical balance coupled with a density kit (Mettler Toledo, model ML204). The morphology anisotropy of the films is characterized using wide-angle X-ray diffraction (see the Supporting Information for details).

# SIMULATION SECTION

Polymer Models. The all-atom MD simulation models were built by BIOVIA Materials Studio, and the consistentvalence force field (CVFF) parameters were adopted.<sup>48</sup> Important simulation parameters are listed in the Supporting Information. The CVFF force field has been successfully used to study thermal transport of different polyelectrolytes in our previous research.  $^{11,18}$  In this model, each polymer chain was built with 8 segments (Figure 1a) with a total chain length of ~160 carbons. The pentiptycene bulky segment ratio was tuned from 0 to 100% with an incremental interval of 12.5%. While the two types of segments are randomly distributed along the backbone of the synthesized copolymers, in our MD model, the two types of segments are separated evenly to simplify simulation processes while providing representative backbone structures, that is, 0%: BBBBBBBB, 12.5%: ABBBBBBB, 25%: ABBBABBB, 37.5%: BBABABAB, 50%: ABABABAB, 62.5%: ABABABAA, 75%: AAABAAAB, 78.5%: AAAAAAA, and 100%: AAAAAAA. By replicating 1 polymer chain into 20 copies, a bulk amorphous polymer model is packed into a simulation box of  $\sim 50 \times 50 \times 50 \text{ Å}^3$ . Depending on the segment ratio, a total number of 10,920 to 18,440 atoms are in the simulation box (Figure 1c).

**Simulation Methods.** All MD simulations were carried using the Large-scale Atomic Molecular Massively Parallel Simulator (LAMMPS) package. The long-range Coulombic force was calculated by the Ewald summation method using the particle–particle particle-mesh (PPPM) algorithm, and the relative force accuracy parameter was set to 0.0001. A single polymer chain was first relaxed under *NPT* (600 K, 1 atm) ensemble until its volume was equilibrated for making replicates. Then, it was replicated to 20 chains. Periodic boundary conditions were applied to *x-*, *y-*, and *z-*directions. After multiple *NVT* (1000–3000 K) heating and *NPT* (300 K, 1 atm) quenching runs, the density of the polymer converged. At the same time, the simulation box was deformed into a cubic shape by running the simulation at high temperatures in

Table 1. Summary of Key Experimental and MD Simulation Results<sup>a</sup>

PPHI	bulky ratio	0%	12.5%	25%	37.5%	50%	62.5%	75%	87.5%	100%
Exp. results	$\rho$ (g/cm <sup>3</sup> )			1.348		1.319		1.288		1.241
	E (GPa)			1.99		2.34		1.96		2.24
	$v_{\rm ave}~({ m m/s})$			1215		1332		1234		1344
	$\rho c_p \left( J/cm^3/K \right)$			1.685		1.873		1.996		1.812
	$\kappa_{\text{out-of-plane}}$ (W/m·K)			$0.111 \pm 0.006$		$0.144 \pm 0.004$		$0.159 \pm 0.013$		$0.148 \pm 0.014$
	$\kappa_{\text{in-plane}} (W/m \cdot K)$			$0.708 \pm 0.004$		$0.809 \pm 0.015$		$0.982 \pm 0.007$		$0.850 \pm 0.001$
	anisotropy			6.38		5.62		6.18		5.74
MD results	$R_{\rm g}$ (Å)	17.8	17.3	20.7	18.7	21.1	19.3	20	21	19.4
	$ ho({ m g/cm^3})$	1.46	1.44	1.40	1.38	1.35	1.34	1.32	1.30	1.29
	$\kappa_{\mathrm{MD}} \; (\mathrm{W/m \cdot K})$	0.159	0.165	0.174	0.189	0.178	0.183	0.194	0.177	0.188

<sup>&</sup>quot;The error bars of thermal conductivity values are the standard deviation of multiple measurements (10 times) of the same sample.

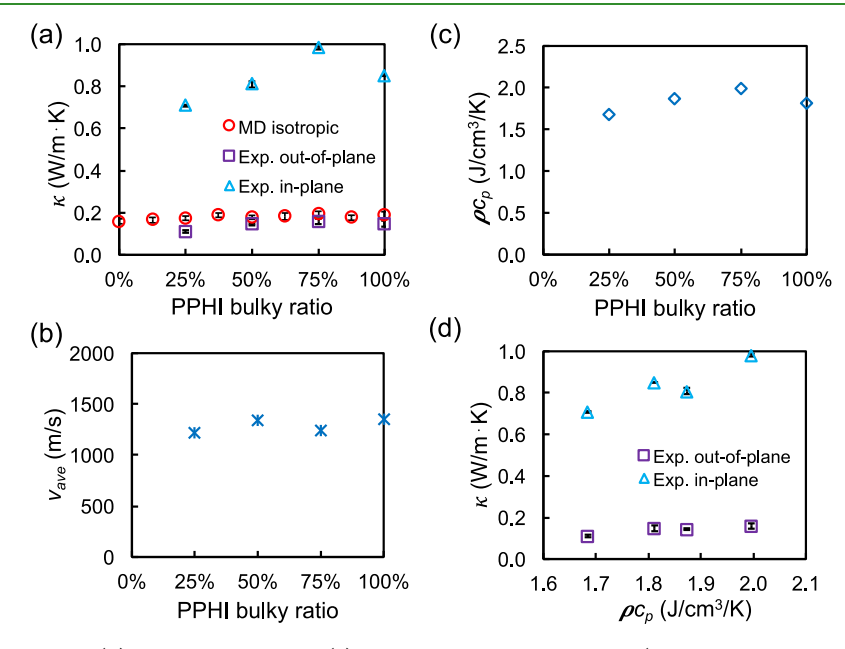


Figure 3. (a) Thermal conductivity, (b) speed of sound, and (c) heat capacity per unit volume (i.e., volumetric heat capacity) as a function of the bulky segment ratio. (d) Thermal conductivity as a function of the heat capacity per unit volume. The error bar of experimental- $\kappa$  is the standard deviation of 10 measurements on the same sample. The error bar of MD- $\kappa$  is the standard deviation of 10 data points from 5 different time periods each after steady state in two ensembles.

an NVT (1000-3000 K) ensemble. The final polymer model was close to a cube with the side length ranging from 50 to 80 Å, which increases as the PPHI bulky ratio increases from 0 to 100%. In order to create an amorphous polymer structure and relax polymer chains completely, we spent more than 50 ns simulation time to relax each polymer model under the NVT (3000 K) ensemble. Figure 2a shows that the average  $R_g$  of the 20 chains for each segment ratio generally converges after ~40 ns. In the end, before the production simulations, the polymer was quenched to 300 K and relaxed under NPT (300 K, 1 atm) ensemble for 1 ns and then in the NVT (300 K) ensemble for 0.5 ns. The chain conformation  $(R_g)$  at 300 K is plotted in Figure 2b, which shows that  $R_{\varphi}$  has a weak positive relation with the ratio of the bulky segment. Figure 2c also shows that the density decreases as the bulky segment ratio increases, and the MD values are less than 4% different from the experimental data. The bulk polymer structure was further characterized by the radial distribution function (RDF). Figure 2d shows an increase trend at ~4 Å on the RDF that involves all atoms, which is due to the increase in aromatic carbon atoms (Figure S1a, Supporting Information). Figure 2d also shows a decrease trend at  $\sim$ 2.9 Å, which is due to the decrease in fluorine atoms

(Figure S1b, Supporting Information). Both of these RDF trends are directly from the change in the ratio of the bulky segment.

The FFV was calculated by both the meshing method<sup>51</sup> and the artificial particle filling method. 52 In the meshing method (Figure S2a, Supporting Information), the simulation box was meshed by a grid size of 0.5 Å. For each grid point, if there was no atom within a cutoff distance  $(r_c)$ , the grid was deemed to be in free volume. Finally, the FFV was calculated as the ratio of the number of grids in free volume to all grids. We compared different  $r_c$  values (1.0, 1.5, and 2.0 Å) for FFV calculations. In the artificial particle filling method (Figure S2b, Supporting Information), a monoatomic gas was filled into the polymer matrix using the grand canonical Monte Carlo (GCMC) simulation,<sup>53</sup> with a Lennard-Jones (LJ) model of  $\varepsilon$  = 0.05 kcal/mol and  $\sigma$  = 1.0 Å describing the artificial gas atom and a chemical potential of  $\mu = -0.1$  kcal/mol. More than 6,000,000 GCMC steps were carried out for particle filling in each model. The volume of artificial gas was calculated by the Voronoi tessellation method<sup>54</sup> at the final GCMC step, and FFV was calculated as the ratio between the total volume of artificial gas and the total volume of the

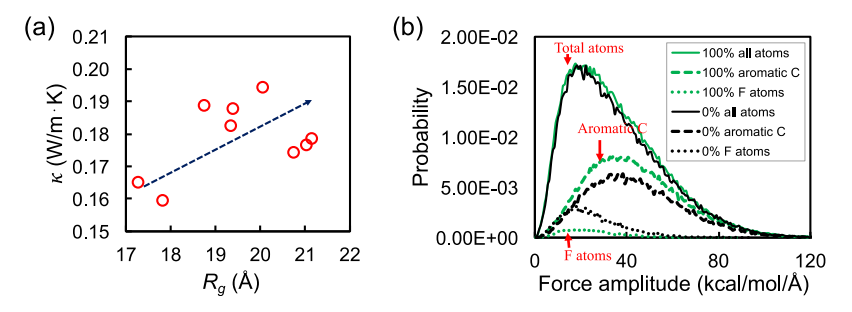


Figure 4. (a) Thermal conductivity as a function of  $R_v$ . (b) Force amplitude histogram on different atoms.

simulation box. This method is referred to as the GCMC method in the following text.

In order to perform the nonequilibrium MD simulations to calculate the thermal conductivity, the polymer box was further replicated in the y-direction (Figure S3a, Supporting Information). A heat source was applied in the middle, and two heat sinks were set at the edges of the simulation box along the y-direction. At steady state, the temperature gradient (Figure S3b, Supporting Information) and heat flux (Figure S3c, Supporting Information) were calculated. Thermal conductivity ( $k_{\rm MD}$ ) was obtained by Fourier's law.

# ■ RESULTS AND DISCUSSION

Thermal Conductivity of PPHI Copolymers. Experimental and MD simulation results from this study are listed in Table 1. Our experimental results of the PPHI copolymer films show that the out-of-plane thermal conductivity is in the range of 0.111-0.159 W/(m·K), and it generally increases with the bulky segment ratio (purple squares in Figure 3a). We also find significant anisotropy in the film thermal conductivity with the in-plane values 5.62-6.38 times the out-of-plane values. The in-plane thermal conductivity also generally increases with the bulky segment ratio, and the highest value reaches 0.982 W/m· K, which is very high for amorphous polymers (blue triangles in Figure 3a). The large anisotropy should be from the film casting, where the surface tension of the solution forces the polymer chains to be more aligned in the in-plane direction, and thus the in-plane heat transfer is more efficient. The anisotropy of the neat polymer film and composite thermal conductivity has been reported previously. Kurabayashi et al. 55 observed a thermal conductivity anisotropy factor of about 4 to 8 at room temperature for spin-casted polyimide polymer films in the thickness range of  $0.5-2.25 \mu m$ . The spin casting applies a large shear to align polymer chains in the in-plane direction. It is interesting to find that our solution-casted films, which do not experience a large shear as those in spin-casting, can also possess a very high anisotropy. For all films, the azimuthal profiles of our wide-angle X-ray diffraction measurements showed intensity variations across all beta angles, which suggested that there were preferred amorphous ordering in the samples (see Figure S8 in the Supporting Information). Since the polymers are confirmed to be amorphous, such ordering is likely from the casting process. Anisotropy of polymer composite films (e.g., carbon nanotube—conjugated polyelectrolyte composites and boron nitride—polymer composites<sup>57</sup>) can be even higher (up to ~200), but it is due to the alignment of the high thermal conductivity fillers in the inplane direction.

Using the measured Young's modulus (E, Table 1), we calculate the speed of sound of our PPHI films via  $v_{ave} = \sqrt{\frac{E}{\rho}}$ ,

where  $\rho$  is the density.<sup>58</sup> While we understand that such calculated speed of sound is not necessarily the same as the propagation speed of higher frequency modes, it should nevertheless provide an indication of whether changing the bulky segment ratio can influence the speed of heat carriers. The speed of sound fluctuates as the bulky segment ratio increases without an obvious trend (Figure 3b). We have additionally calculated the transverse and longitudinal speeds of sound from MD simulations, which also do not show any trend as a function of the bulky segment ratio (see Supporting Information, Figure S7). The density of the PPHI film decreases as the bulky segment ratio increases (Figure 2c), which is opposite to the trend of thermal conductivity. However, if we consider Kittel's simple model for thermal conductivity of amorphous materials,  $\kappa = cvl_1^{59}$  it is the volumetric heat capacity, instead of density, that directly impacts thermal conductivity (Figure 3c,d), although they are correlated. Usually, volumetric heat capacity has a positive relation with density, but for PPHI, this is not the case, where the density decreases but the volumetric heat capacity increases as the bulky segment ratio increases. The reason is that not all vibrational modes, which are proportional to the atom number density, are excited at room temperature. Highfrequency modes are not excited according to Bose-Einstein distribution at room temperature. To take into account this quantum effect, modifications have been proposed to reduce heat carrying degrees of freedom by ignoring modes related to certain strong chemical bonds, where only two-thirds of the total atoms, excluding hydrogen atoms, are considered to contribute to heat capacity. 16,18 However, this still does not give atom number density (Figure S4) the same trend as that of heat capacity when the copolymer segment ratio changes. The number density of aromatic carbon atoms, however, increases with the bulky segment ratio since many of them are part of the bulky segment. It is possible that vibrational modes related to the aromatic ring structure in the bulky segment cover a lower frequency region better than its counterpart -CF<sub>3</sub> segment, and thus these low-frequency modes are more excited at room temperature and contribute to heat capacity.

In the MD simulations, the modeled polymers are amorphous and isotropic because of the way they are prepared. MD results show that the isotropic thermal conductivity of the bulk amorphous PPHI copolymers is between 0.15 and 0.20 W/m·K (red circles in Figure 3a), which falls into the range of common conjugated polymers (0.1–0.4 W/m·K).<sup>33</sup> It is also reasonable that the values are also in-between the in-plane and out-of-plane thermal conductivity values measured from our experiments. In addition, we also observe a generally increasing trend in thermal conductivity from MD with the increase of

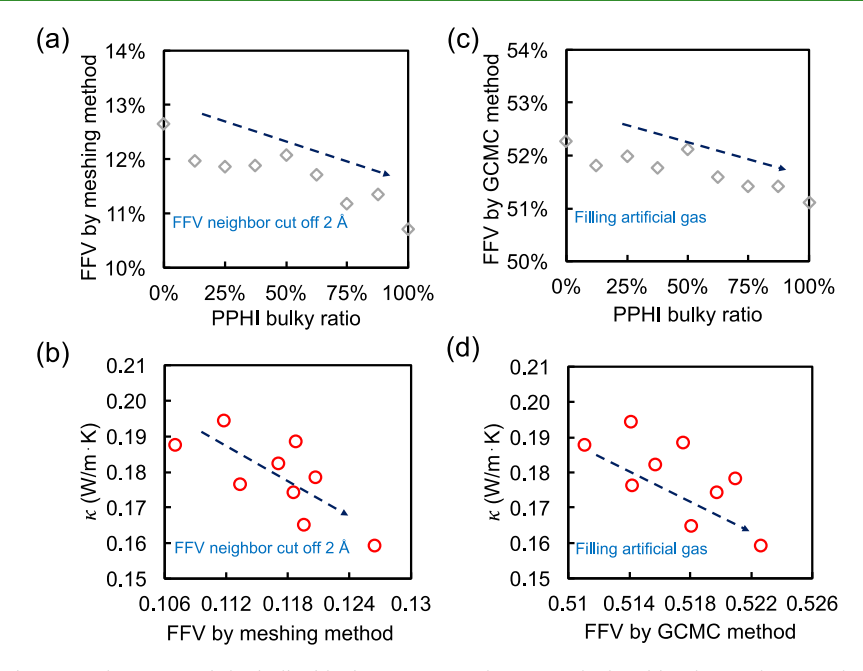


**Figure 5.** (a) Relationship between the FFV and the bulky block ratio, using the FFV calculated by the meshing method with a neighbor cutoff at 2.0 Å. (b) Negative relationship between thermal conductivity and the FFV. (c) Confirmation of the relationship between the bulky block ratio and the FFV by the GCMC method. (d) Confirmation of the negative relationship between thermal conductivity and the FFV by the GCMC method.

the bulky segment ratio, which is consistent with the experimental results.

Effects from the PPHI Bulky Segment. The above observation about thermal conductivity correlating well with the observed heat capacity is phenomenological based on Kittel's simplified model from the kinetic theory. However, in polymers, thermal transport along the chain backbone and across chains are drastically different, which makes thermal conductivity in the amorphous polymer closely related to chain conformation. Previous studies have shown that thermal conductivity generally has a positive correlation with  $R_{\rm g}$ . 12,19,26 A larger  $R_{\rm g}$  means that the polymer chains are more spatially extended, and thus thermal transport along the chain backbone can reach longer distances, making thermal transport more efficient. Although we cannot quantitatively analyze the molecular conformation in our experimental samples, the fact that our MD-calculated density and thermal conductivity share the same trends as those of the experimental counterparts allows us to leverage the MD results to shed light on the correlation between the molecular-level characteristics and thermal conductivity.

In general, the results from our MD simulations show a roughly positive relationship between thermal conductivity and  $R_{g}$  (Figure 4a). As previously shown in Figure 2c, as the bulky segment ratio increases,  $R_g$  increases. This generally agrees with the fact that bulky groups make the chain stiffer,<sup>30</sup> and thus there is higher  $R_g$ . In addition, at the molecular level, thermal transport is achieved by atoms doing work to one another via interatomic forces. 60 By examining the atomic forces on the aromatic carbon atoms, it is evident that these atoms experience the largest forces among all atoms, and the forces they experience are much larger than those on the fluorine atoms in the -CF<sub>3</sub> substituent group (Figure 4b). Figure 4b shows the histograms of the forces on these atoms for 0% (black) and 100% (green) bulky segment ratios. When the bulky segment ratio increases, the strong force on aromatic carbon atoms at 40 kcal/mol/Å becomes more populated,

while the weaker force on fluorine atoms at 20 kcal/mol/Å decreases. As a result, when the number of bulky groups is greater, thermal conductivity can be enhanced.

Role of Free Volume Effect. FFV is defined as the percentage of unoccupied space in a given polymer volume. It is calculated as the ratio of the free volume and the specific volume determined from the density. In the PPHI copolymers studied here, the pentiptycene-based segment is much bulkier than the -CF<sub>3</sub>-based segment (Figure 1a). It is thus expected that increasing the bulky segment ratio will increase the free volume of the polymer typically accompanying the decreased polymer density. While the results from both FFV calculation methods show a decreasing trend in FFV as the bulky segment ratio increases (Figure 5a,b), which was also previously seen in the triptycene-based polymers. 36,37 Figure 5a shows that using a cutoff of 2 Å, the simulated FFV decreases slightly from  $\sim$ 12.6 to  $\sim$ 10.7% as the bulky segment ratio increases from 0 to 100%. By applying different cutoff distances in the meshing method, the FFV increases with a smaller cutoff (Figure S5a,b in the Supporting Information), but the decreasing trend of FFV remains the same. Figure 5b also shows that thermal conductivity displays a generally decreasing trend when the FFV increases because free volume voids cannot transfer heat. These findings provide another reason for thermal conductivity increasing with the increase in the bulky segment ratio (Figure 3). The FFV is also calculated by the GCMC method (details, see Figure S5c,d, Supporting Information). The FFV values determined by the GCMC method is at ~50% because the artificial LJ gas is small with  $\varepsilon = 0.05$  kcal/mol and  $\sigma = 1.0$  Å. Such a small artificial gas can fill all possible empty space in the polymer, and the trends of decreasing FFV with the increasing bulky segment ratio stay the same (Figure 5c). It is important that the FFV by the GCMC method (Figure 5d) confirms the trend of decrease in thermal conductivity with increasing FFV.

# CONCLUSIONS

In this paper, we use experiments and MD simulations to study thermal conductivity of PPHI copolymers. The effects of the PPHI bulky segment ratio on polymer thermal conductivity are investigated. Both experimental and MD results show that thermal diffusivity increases with the PPHI bulky segment ratio. Due to the chain alignment in the in-plane direction in our experimental samples, the in-plane thermal conductivity is significantly higher than the out-of-plane direction. Experimental results show that the volumetric heat capacity increases with the bulky segment ratio, which in turn increases the thermal conductivity. MD results further show that the bulky segment helps increase the  $R_{\sigma}$  of polymer chains and the amount of large interatomic forces related to the aromatic carbon in the bulky segment, both leading to increasing thermal conductivity. In addition, we also find that the FFV in the PPHI copolymers decreases as the bulky segment ratio increases, and thermal conductivity decreases as the FFV increases.

#### ASSOCIATED CONTENT

# Supporting Information

The Supporting Information is available free of charge at https://pubs.acs.org/doi/10.1021/acsapm.1c00128.

Simulation models and force field parameters; simulation methods in detail; and additional experimental and simulation results (PDF)

# **■** AUTHOR INFORMATION

# **Corresponding Author**

Tengfei Luo — Department of Aerospace and Mechanical Engineering and Department of Chemical and Biomolecular Engineering, University of Notre Dame, Notre Dame, Indiana 46556, United States; ⊚ orcid.org/0000-0003-3940-8786; Phone: (574) 631-9683; Email: tluo@nd.edu

# **Authors**

- Xingfei Wei Department of Aerospace and Mechanical Engineering, University of Notre Dame, Notre Dame, Indiana 46556, United States
- Zihan Huang Department of Chemical and Biomolecular Engineering, University of Notre Dame, Notre Dame, Indiana 46556, United States
- Stephen Koch Department of Aerospace and Mechanical Engineering, University of Notre Dame, Notre Dame, Indiana 46556, United States
- Massimiliano Zamengo Department of Materials Science and Engineering, School of Materials and Chemical Technology, Tokyo Institute of Technology, Tokyo 152-8550, Iapan
- Yichen Deng Department of Mechanical and Industrial Engineering Department, Northeastern University, Boston 02115, Massachusetts, United States
- Marilyn L. Minus Department of Mechanical and Industrial Engineering Department, Northeastern University, Boston 02115, Massachusetts, United States
- Junko Morikawa Department of Materials Science and Engineering, School of Materials and Chemical Technology, Tokyo Institute of Technology, Tokyo 152-8550, Japan; orcid.org/0000-0002-9530-9478

Ruilan Guo — Department of Chemical and Biomolecular Engineering, University of Notre Dame, Notre Dame, Indiana 46556, United States; orcid.org/0000-0002-3373-2588

Complete contact information is available at: https://pubs.acs.org/10.1021/acsapm.1c00128

#### **Notes**

The authors declare no competing financial interest.

# ACKNOWLEDGMENTS

The authors acknowledge the financial support from DuPont Young Professor Award and the Dorini Family endowed professorship. Z.H. and R.G. acknowledge the support from the financial support from the National Science Foundation under the cooperative agreement no. EEC-1647722, an Engineering Research Center for the Innovative and Strategic Transformation of Alkane Resources (CISTAR). This computation was supported in part by the University of Notre Dame, Center for Research Computing, and NSF through XSEDE resources provided by TACC Stampede-II under grant number TG-CTS100078. J.M. acknowledges financial support from the Japan Society for the Promotion of Science (JSPS), Japan KAKENHI Grant number 20H04663, and JST CREST Grant Number JPMJCR19I3.

#### REFERENCES

- (1) Henry, A. Thermal transport in polymers. *Annu. Rev. Heat Transfer* **2013**, *17*, 485–520.
- (2) Cahill, D. G.; Braun, P. V.; Chen, G.; Clarke, D. R.; Fan, S.; Goodson, K. E.; Keblinski, P.; King, W. P.; Mahan, G. D.; Majumdar, A.; Maris, H. J.; Phillpot, S. R.; Pop, E.; Shi, L. Nanoscale thermal transport. II. 2003-2012. *Appl. Phys. Rev.* **2014**, *1*, 011305.
- (3) Mehra, N.; Mu, L.; Ji, T.; Yang, X.; Kong, J.; Gu, J.; Zhu, J. Thermal transport in polymeric materials and across composite interfaces. *Appl. Mater. Today* **2018**, *12*, 92–130.
- (4) Klonos, P. A.; Peoglos, V.; Bikiaris, D. N.; Kyritsis, A. Rigid Amorphous Fraction and Thermal Diffusivity in Nanocomposites Based on Poly(l-lactic acid) Filled with Carbon Nanotubes and Graphene Oxide. *J. Phys. Chem. C* **2020**, *124*, 5469–5479.
- (5) Juangsa, F. B.; Ryu, M.; Morikawa, J.; Nozaki, T. Interfacial region effect on thermal conductivity of silicon nanocrystal and polystyrene nanocomposites. *Plasma Processes Polym.* **2020**, 17, 1900212.
- (6) Luo, T.; Chen, G. Nanoscale heat transfer from computation to experiment. *Phys. Chem. Chem. Phys.* **2013**, *15*, 3389–3412.
- (7) Pang, Y.; Zhang, J.; Ma, R.; Qu, Z.; Lee, E.; Luo, T. Solar-Thermal Water Evaporation: A Review. ACS Energy Lett. 2020, 5, 437–456.
- (8) Liu, J.; Yang, R. Tuning the thermal conductivity of polymers with mechanical strains. *Phys. Rev. B: Condens. Matter Mater. Phys.* **2010**, *81*, 174122.
- (9) Zhang, T.; Luo, T. Morphology-influenced thermal conductivity of polyethylene single chains and crystalline fibers. *J. Appl. Phys.* **2012**, *112*, 094304.
- (10) Zhang, T.; Luo, T. Role of chain morphology and stiffness in thermal conductivity of amorphous polymers. *J. Phys. Chem. B* **2016**, 120, 803–812.
- (11) Wei, X.; Luo, T. Role of Ionization in Thermal Transport of Solid Polyelectrolytes. *J. Phys. Chem. C* **2019**, *123*, 12659–12665.
- (12) Wei, X.; Luo, T. Chain length effect on thermal transport in amorphous polymers and a structure-thermal conductivity relation. *Phys. Chem. Chem. Phys.* **2019**, *21*, 15523–15530.
- (13) Ouyang, Y.; Zhang, Z.; Xi, Q.; Jiang, P.; Ren, W.; Li, N.; Zhou, J.; Chen, J. Effect of boundary chain folding on thermal conductivity of lamellar amorphous polyethylene. *RSC Adv.* **2019**, *9*, 33549–33557.

- (14) Shen, S.; Henry, A.; Tong, J.; Zheng, R.; Chen, G. Polyethylene nanofibres with very high thermal conductivities. *Nat. Nanotechnol.* **2010**, *5*, 251–255.
- (15) Henry, A.; Chen, G.; Plimpton, S. J.; Thompson, A. 1D-to-3D transition of phonon heat conduction in polyethylene using molecular dynamics simulations. *Phys. Rev. B: Condens. Matter Mater. Phys.* **2010**, 82, 144308.
- (16) Xie, X.; Yang, K.; Li, D.; Tsai, T.; Shin, J.; Braun, P. V.; Cahill, D. G. High and low thermal conductivity of amorphous macromolecules. *Phys. Rev. B* **2017**, *95*, 035406.
- (17) Xie, X.; Li, D.; Tsai, T.-H.; Liu, J.; Braun, P. V.; Cahill, D. G. Thermal Conductivity, Heat Capacity, and Elastic Constants of Water-Soluble Polymers and Polymer Blends. *Macromolecules* **2016**, 49, 972–978.
- (18) Wei, X.; Ma, R.; Luo, T. Thermal Conductivity of Polyelectrolytes with Different Counterions. *J. Phys. Chem. C* **2020**, 124, 4483–4488.
- (19) Wei, X.; Zhang, T.; Luo, T. Chain conformation-dependent thermal conductivity of amorphous polymer blends: the impact of inter- and intra-chain interactions. *Phys. Chem. Chem. Phys.* **2016**, *18*, 32146–32154.
- (20) Lu, T.; Kim, K.; Li, X.; Zhou, J.; Chen, G.; Liu, J. Thermal transport in semicrystalline polyethylene by molecular dynamics simulation. *J. Appl. Phys.* **2018**, *123*, 015107.
- (21) Zhang, T.; Luo, T. High-contrast, reversible thermal conductivity regulation utilizing the phase transition of polyethylene nanofibers. *ACS Nano* **2013**, *7*, 7592–7600.
- (22) He, J.; Kim, K.; Wang, Y.; Liu, J. Strain effects on the anisotropic thermal transport in crystalline polyethylene. *Appl. Phys. Lett.* **2018**, *112*, 051907.
- (23) Zhou, J.; Xi, Q.; He, J.; Xu, X.; Nakayama, T.; Wang, Y.; Liu, J. Thermal resistance network model for heat conduction of amorphous polymers. *Phys. Rev. Mater.* **2020**, *4*, 015601.
- (24) Nieto Simavilla, D.; Sgouros, A. P.; Vogiatzis, G. G.; Tzoumanekas, C.; Georgilas, V.; Verbeeten, W. M. H.; Theodorou, D. N. Molecular Dynamics Test of the Stress-Thermal Rule in Polyethylene and Polystyrene Entangled Melts. *Macromolecules* **2020**, 53, 789–802
- (25) Zhang, Z.; Ouyang, Y.; Cheng, Y.; Chen, J.; Li, N.; Zhang, G. Size-dependent phononic thermal transport in low-dimensional nanomaterials. *Phys. Rep.* **2020**, *860*, 1–26.
- (26) Wei, X.; Luo, T. The effect of the block ratio on the thermal conductivity of amorphous polyethylene-polypropylene (PE-PP) diblock copolymers. *Phys. Chem. Chem. Phys.* **2018**, *20*, 20534–20539.
- (27) Wei, X.; Wang, Z.; Tian, Z.; Luo, T. Thermal Transport in Polymers: A Review. **2020**, arXiv:2009.09430. arXiv preprint.
- (28) Guo, Z.; Lee, D.; Liu, Y.; Sun, F.; Sliwinski, A.; Gao, H.; Burns, P. C.; Huang, L.; Luo, T. Tuning the thermal conductivity of solar cell polymers through side chain engineering. *Phys. Chem. Chem. Phys.* **2014**, *16*, 7764–7771.
- (29) Zhang, T.; Xu, J.; Luo, T. Extremely High Thermal Conductivity of Aligned Polyacetylene Predicted using First-Principles-Informed United-Atom Force Field. 2020, arXiv:2009.13708. arXiv preprint.
- (30) Zhang, T.; Wu, X.; Luo, T. Polymer nanofibers with outstanding thermal conductivity and thermal stability: Fundamental linkage between molecular characteristics and macroscopic thermal properties. *J. Phys. Chem. C* **2014**, *118*, 21148–21159.
- (31) Zhang, Z.; Ouyang, Y.; Guo, Y.; Nakayama, T.; Nomura, M.; Volz, S.; Chen, J. Hydrodynamic phonon transport in bulk crystalline polymers. *Phys. Rev. B* **2020**, *102*, 195302.
- (32) Singh, V.; Bougher, T. L.; Weathers, A.; Cai, Y.; Bi, K.; Pettes, M. T.; McMenamin, S. A.; Lv, W.; Resler, D. P.; Gattuso, T. R.; Altman, D. H.; Sandhage, K. H.; Shi, L.; Henry, A.; Cola, B. A. High thermal conductivity of chain-oriented amorphous polythiophene. *Nat. Nanotechnol.* **2014**, *9*, 384–390.
- (33) Xu, X.; Zhou, J.; Chen, J. Thermal Transport in Conductive Polymer-Based Materials. *Adv. Funct. Mater.* **2020**, *30*, 1904704.

- (34) Xu, Y.; Wang, X.; Zhou, J.; Song, B.; Jiang, Z.; Lee, E. M. Y.; Huberman, S.; Gleason, K. K.; Chen, G. Molecular engineered conjugated polymer with high thermal conductivity. *Sci. Adv.* **2018**, *4*, No. eaar3031.
- (35) Guo, R.; Sanders, D. F.; Smith, Z. P.; Freeman, B. D.; Paul, D. R.; McGrath, J. E. Synthesis and characterization of thermally rearranged (TR) polymers: effect of glass transition temperature of aromatic poly(hydroxyimide) precursors on TR process and gas permeation properties. *J. Mater. Chem. A* **2013**, *1*, 6063–6072.
- (36) Sanders, D. F.; Smith, Z. P.; Guo, R.; Robeson, L. M.; McGrath, J. E.; Paul, D. R.; Freeman, B. D. Energy-efficient polymeric gas separation membranes for a sustainable future: A review. *Polymer* **2013**. *54*. 4729–4761.
- (37) Luo, S.; Liu, Q.; Zhang, B.; Wiegand, J. R.; Freeman, B. D.; Guo, R. Pentiptycene-based polyimides with hierarchically controlled molecular cavity architecture for efficient membrane gas separation. *J. Membr. Sci.* **2015**, *480*, 20–30.
- (38) Luo, S.; Wiegand, J. R.; Kazanowska, B.; Doherty, C. M.; Konstas, K.; Hill, A. J.; Guo, R. Finely tuning the free volume architecture in iptycene-containing polyimides for highly selective and fast hydrogen transport. *Macromolecules* **2016**, *49*, 3395–3405.
- (39) Luo, S.; Zhang, Q.; Zhu, L.; Lin, H.; Kazanowska, B. A.; Doherty, C. M.; Hill, A. J.; Gao, P.; Guo, R. Highly selective and permeable microporous polymer membranes for hydrogen purification and CO2 removal from natural gas. *Chem. Mater.* **2018**, *30*, 5322–5332.
- (40) Sumirat, I.; Ando, Y.; Shimamura, S. Theoretical consideration of the effect of porosity on thermal conductivity of porous materials. *J. Porous Mater.* **2006**, *13*, 439–443.
- (41) Novais, R. M.; Seabra, M. P.; Labrincha, J. A. Ceramic tiles with controlled porosity and low thermal conductivity by using poreforming agents. *Ceram. Int.* **2014**, *40*, 11637–11648.
- (42) Dettori, R.; Melis, C.; Cartoixà, X.; Rurali, R.; Colombo, L. Model for thermal conductivity in nanoporous silicon from atomistic simulations. *Phys. Rev. B* **2015**, *91*, 054305.
- (43) Tarkhanyan, R. H.; Niarchos, D. G. Reduction in lattice thermal conductivity of porous materials due to inhomogeneous porosity. *Int. J. Therm. Sci.* **2013**, *67*, 107–112.
- (44) Sundarram, S. S.; Li, W. On thermal conductivity of micro- and nanocellular polymer foams. *Polym. Eng. Sci.* **2013**, *53*, 1901–1909.
- (45) Miyata, T.; Inaki, K.; Morikawa, J.; Satoto, R.; Hashimoto, T. Effects of copolyester/polycarbonate blend composition on the thermal diffusivity of dye transfer printing. *J. Appl. Polym. Sci.* **2004**, 92, 72–76.
- (46) Sawada, T.; Tsuruoka, T.; Ueda, N.; Marubayashi, H.; Nojima, S.; Morikawa, J.; Serizawa, T. Thermally conductive molecular assembly composed of an oligo (ethylene glycol)-modified filamentous virus with improved solubility and resistance to organic solvents. *Polym. J.* **2020**, *52*, 803–811.
- (47) Hashimoto, M.; Imoto, H.; Matsukawa, K.; Naka, K. Coexistence of Optical Transparency, Hydrophobicity, and High Thermal Conductivity in Beads-on-String-Shaped Polyureas Induced by Disordered Hydrogen-Bond Networks. *Macromolecules* **2020**, *53*, 2874–2881.
- (48) Materials Studio Software. Dassault Systèmes BIOVIA, Materials Studio, Version 8, Dassault Systèmes: San Diego, 2014.
- (49) Plimpton, S.; Crozier, P.; Thompson, A. LAMMPS-large-scale Atomic/molecular Massively Parallel Simulator, http://lammps.sandia.gov. Sandia National Laboratories 2007, 18.
- (50) Hockney, R. W.; Eastwood, J. W. Computer simulation using particles. In *Reference book for the models of the N-body problem with pseudo-particle methods*; Adam Hilger, 1989.
- (51) Zanuy, D.; León, S.; Alemán, C.; Munoz-Guerra, S. Molecular simulation of gas solubilities in crystalline poly( $\alpha$ -alkyl- $\beta$ -?-aspartate)s. *Polymer* **2000**, *41*, 4169–4177.
- (52) Kupgan, G.; Demidov, A. G.; Colina, C. M. Plasticization behavior in polymers of intrinsic microporosity (PIM-1): A simulation study from combined Monte Carlo and molecular dynamics. *J. Membr. Sci.* **2018**, *565*, 95–103.

- (53) Frenkel, D.; Smit, B. Understanding Molecular Simulation: from Algorithms to Applications; Elsevier, 2001.
- (54) Rycroft, C. Voro++: A Three-Dimensional Voronoi Cell Library in C++, 2009.
- (55) Kurabayashi, K.; Asheghi, M.; Touzelbaev, M.; Goodson, K. E. Measurement of the thermal conductivity anisotropy in polyimide films. *J. Microelectromech. Syst.* **1999**, *8*, 180–191.
- (56) Mai, C.-K.; Liu, J.; Evans, C. M.; Segalman, R. A.; Chabinyc, M. L.; Cahill, D. G.; Bazan, G. C. Anisotropic thermal transport in thermoelectric composites of conjugated polyelectrolytes/single-walled carbon nanotubes. *Macromolecules* **2016**, *49*, 4957–4963.
- (57) Wu, Y.; Xue, Y.; Qin, S.; Liu, D.; Wang, X.; Hu, X.; Li, J.; Wang, X.; Bando, Y.; Golberg, D.; Chen, Y.; Gogotsi, Y.; Lei, W. BN nanosheet/polymer films with highly anisotropic thermal conductivity for thermal management applications. *ACS Appl. Mater. Interfaces* **2017**, *9*, 43163–43170.
- (58) Sinha, M.; Buckley, D. J. Acoustic properties of polymers. In *Physical Properties of Polymers Handbook*; Springer, 2007; pp 1021–1031. DOI: 10.1007/978-0-387-69002-5 60
- (59) Chen, G. Nanoscale Energy Transport and Conversion: A Parallel Treatment of Electrons, Molecules, Phonons, and Photons; Oxford University Press, 2005.
- (60) Domingues, G.; Volz, S.; Joulain, K.; Greffet, J. Heat transfer between two nanoparticles through near field interaction. *Phys. Rev. Lett.* **2005**, *94*, 085901.